RSC Advances

PAPER

View Article Online
View Journal | View Issue

Cite this: *RSC Adv.*, 2023, **13**, 9091

Superior hydrogen performance of *in situ* formed carbon modified MgH_2 composites

Ying Cheng,[ac] Wei Zhang, *[b] Jing Chen,[c] Jiachen Wang,[a] Pei Pei[a] and Fengxin Li[a]

Received 12th January 2023
Accepted 28th February 2023

DOI: 10.1039/d3ra00232b

rsc.li/rsc-advances

The MgH_2-carbonic combustion product of the anthracene (CCPA) composite was synthesized by hydrogen combustion and mechanically ball-milled method to simultaneously achieve confinement by the *in situ* formed amorphous carbon. The amorphous carbon derived from the carbonic combustion product of anthracene in the MgH_2-CCPA composite led to a significant increase in hydrogen sorption characteristics. The onset dehydrogenation temperature for the MgH_2-CCPA composite was reduced to 589 K, which was 54 K less than that of pure milled MgH_2. Regarding dehydrogenation kinetics, the MgH_2-CCPA composite could release 5.933 wt% H_2 within 3000 s at 623 K, while only 3.970 wt% H_2 was liberated from the as-milled MgH_2 within 3000 s at the same temperature. The MgH_2-CCPA composite also exhibited excellent hydrogenation characteristics, absorbing 3.246 wt% of hydrogen within 3000 s at 423 K, which was three times higher than 0.818 wt% uptaken by the pure MgH_2. The apparent activation energy (E_a) for the dehydrogenation of the MgH_2-CCPA composite was significantly reduced from 161.1 kJ mol^{-1} to 77.5 kJ mol^{-1}. The notable improvement in sorption kinetics of the MgH_2-CCPA nanocomposite is ascribed to the *in situ* formed amorphous carbon during the hydrogenation/dehydrogenation process.

1 Introduction

The great challenges we face from energy crises and environmental problems force us to seek alternative energies to replace the traditional fossil fuels.[1–3] Hydrogen is an ideal energy source possessing the advantages of abundant resources, non-toxicity and environment friendliness and is expected to be a promising candidate for the new generation renewable vectors.[4,5] Moreover, the heat combustion of hydrogen is about three times higher than that of fossil fuel, and its conspicuous advantage makes it an attractive choice among other renewable energy sources.[6,7] Actually, there is still a long way to realize the huge utilization of hydrogen energy due to its efficient and safe storage manner.[8,9] The traditional high-pressure compressed and low-temperature cryogenic liquid hydrogen storage methods, which involve a high standard of required equipment and maintenance cost, are not suitable for the large-scale application in the on-board vehicles. Among the various solid-state hydrogen storage materials, Mg-based materials (especially MgH_2) have been considered the conspicuous storage materials due to their apparent virtue, high hydrogen capacity, excellent reversibility as well as an abundant reserve. However, owing to the stable thermodynamics and sluggish hydrogen sorption kinetics, the practical application of MgH_2 in stationary and mobile energy storage applications is still unsatisfying.

Extensive strategies, including reducing the particle size, ball milling, and alloying with transition metals or non-transition metals, have been studied to alter hydrogen sorption thermodynamics and kinetics of MgH_2.[10] Among various investigations, carbon and carbon-based materials with high porosity and abundant defects are proven to exhibit excellent performance for the improvement of hydrogen sorption kinetics and reduce the desorption temperature. Zhang *et al.*[11] employed a facile chemical solid state method to *in situ* grow MgH_2 nanoparticles with various carbon materials and further compared the effect of different carbon materials on the hydrogen performance of MgH_2, indicating that MgH_2@CSC composites had excellent hydrogen absorption/desorption performance with a release of 5.4 wt% hydrogen within 10 min at 325 °C and absorbed 5.0 wt% hydrogen within 5 min at 250 °C. Zhao *et al.*[12] synthesized the core–shell CoNi@C bimetallic nanoparticles through hydrothermal and calcination reduction methods and further studied the catalytic effect on the hydrogen sorption of MgH_2. The experimental results indicated that the CoNi@C catalyst showed a decrease in the decomposition temperature of MgH_2 and enhanced sorption kinetics, which was attributed to the reversible phase transitions of Mg_2Co and Mg_2Ni as well as the confinement effect of

[a]*Department of Environmental Engineering, Hebei University of Environmental Engineering, Qinhuangdao, 066102, PR China*

[b]*Hebei Key Laboratory of Applied Chemistry, School of Environmental and Chemical Engineering, Yanshan University, Qinhuangdao 066004, PR China. E-mail: zhangweihh@ysu.edu.cn; Tel: +86-010-8387744*

[c]*Hebei Key Laboratory of Agroecological Safety, Hebei University of Environmental Engineering, Qinhuangdao, 066102, PR China*

the carbon shell. Zhang *et al.*[13] reported the hydrogenation/dehydrogenation performances of MgH_2 were enhanced after being catalyzed by the flower-like TiO_2@C nanostructures. The MgH_2-TiO_2@C composite could desorb 6.0 wt% of hydrogen at 250 °C within 7 min and 4.86 wt% of hydrogen at 225 °C within 60 min. The prominent hydrogen storage property is mainly due to the special structure and the two-phase coexistence of TiO_2 and amorphous carbon. Rud *et al.*[14] also reported that carbon materials added to magnesium during the reactive ball milling process led to essential shortening of the hydrogenation time in comparison with elemental magnesium. Carbon material, such as porous hollow carbon nanospheres, was proven to improve the hydrogen storage properties in carbon-based nanoconfined $LiBH_4$ systems.[15] Meanwhile, carbon material also played a vital role in the electrochemical field. As mentioned above, it is worth noting that carbon materials are beneficial to reduced decomposition temperature and improved hydrogen sorption kinetics. Zhu *et al.*[16] confirmed that amorphous alloys possess higher discharge capacity than crystalline alloys. Nevertheless, the catalysts were *in situ* formed in the Mg matrix, and these uniformly dispersed catalysts show better catalytic effects than the catalysts added by ball milling.[17] Therefore, introducing carbon-based material to the amorphous composites through the *in situ* formed method is a vital modification strategy for the improved hydrogen sorption properties on account of the varied morphology and excellent thermal conductivity.

Illuminated by the above research studies, a novel strategy of amorphous carbon synthesized through the *in situ* formed method is proposed. Anthracene with 94 wt% C is identified as the origin of the carbon resources. The amorphous carbon with MgH_2 is prepared by the hydrogen combustion synthesis method, and the hydrogen dynamic kinetics and thermodynamic properties for the MgH_2 with amorphous carbon synthesized through the *in situ* formed method are presented, and their catalytic mechanism is also investigated systematically.

2 Experimental

2.1 Preparation of MgH_2-CCPA composites

The original Mg powder with a purity of 99.9% was purchased from Sinopharm Chemical Reagent co., Ltd. Anthracene was commercially purchased from the Macklin company. All the reactants are utilized without further purification. The Mg and anthracene were manually and mechanically stirred together with a molar ratio of 3 : 1, and the mixed sample was placed in the ball mill vial accompanied by the ball-to-powder weight ratio of 40 : 1. To prevent the rising milling temperature, the ball mill worked in one direction for 30 min, rested for 15 min, and then turned in the other direction for 30 min. After finishing the ball-milling process, the samples were calcined in a tube furnace in Ar atmosphere from room temperature to 550 °C with the heating rate of 5 °C min^{-1} and heated at 550 °C for 2 h, and the Mg-carbonic combustion product of anthracene (CCPA) was prepared. The Mg-CCPA powder was hydrogenated at 400 °C for 15 h under a pressure of 4.0 MPa. When the temperature was brought down to room temperature, the ball mill process was subsequently continued in one direction for 30 min, rested for 15 min, and then turned in the other direction for 30 min. The MgH_2-CCPA powder was successfully obtained by repeating the "hydrogenation-ball milling" process three times. The pure MgH_2 was successfully obtained by repeating the above "hydrogenation-ball milling" process three times. The purpose of the above operation is to promote the Mg powder to be fully converted into MgH_2. The hydrogen absorption/desorption of Mg is so poor, which belongs to the hydrogenation process of Mg powder. Pure Mg is fully converted to MgH_2 through the "hydrogenation-ball milling" process three times. Moreover, ball-milling treatment can also effectively reduce the crystallite and particle size of powder samples. The samples were handled in an Ar-filled glove box to prevent oxidation and humidity.

2.2 Characterization

X-ray diffraction (XRD) analyses were performed on SmartLab high resolution X-ray diffractometer (made by Rigaku company) with Cu Kα radiation at 40 kV, 40 mA. The 2θ range varied from 10° to 80° with a scanning rate of 5° min^{-1}. The corresponding XRD data were verified and analyzed by MID Jade 6.0 software. Field emission scanning electron microscope (SEM, FEI-NOVA NANO 230) with an energy dispersive spectroscope (EDS, Oxford EDS X-Max50) was employed to characterize the microstructure and morphology of the material. The constitution of the composite was further confirmed by Raman characterization using an in Via ReflexRenishaw spectrometer, and the data were collected in the anti-Stokes range of 100–2000 cm^{-1}. The He–Gd laser was utilized to excite the sample with the excitation wavelength of 532 nm. The element distribution of the sample was detected by X-ray photoelectron spectroscopy (XPS).

The temperature-programmed desorption (TPD) analysis and the hydrogen sorption kinetic experiments were assessed in a homemade Sieverts-type pressure–composition–temperature (PCT) apparatus (made by GRINM Co., China). The intrinsic hydrogen desorption property of the sample was determined by the TPD test with the heating rate of 10 K min^{-1} from room temperature to 873 K under a pressure of 0.001 MPa. Especially, the hydrogen sorption performance for the composite was conducted by a PCT apparatus under 3.0 MPa for absorption at 423 K, 473 K, 523 K, and 0.001 MPa for desorption at 575 K, 598 K, and 623 K, respectively. The desorption properties at different heating rates of 5 K min^{-1}, 10 K min^{-1}, 15 K min^{-1}, and 20 K min^{-1} were investigated by differential scanning calorimetry (DSC).

3 Results and discussion

3.1 Characterization of the prepared MgH_2-CCPA composite

The phase composition of the as-synthesized MgH_2-CCPA composite is identified by XRD and Raman studies. XRD pattern of the prepared MgH_2-CCPA composite is shown in Fig. 1a. A noticeable feature is that the prepared MgH_2-CCPA composite has sharp diffraction peaks, and the dominant diffraction peaks centered at 27.95° (110), 35.74° (101), 39.86° (200), 54.62° (211), 57.75° (220), 61.34° (400), 65.34° (310), 68.77° (112), and 75.73°

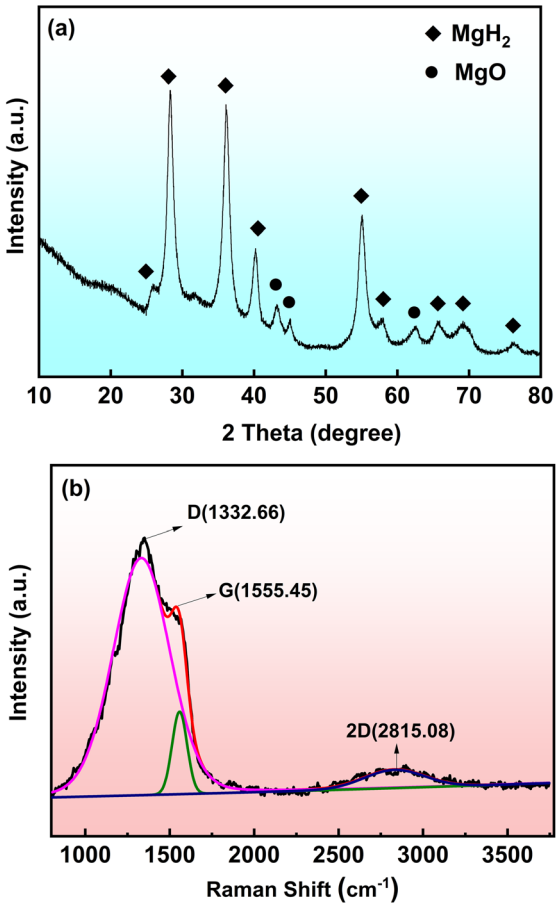

Fig. 1 (a) XRD pattern and (b) Raman spectra of the as-synthesized MgH_2-CCPA composite.

(202) ascribed well with the standard card MgH_2 (PDF#12-0697). There is a weak diffraction peak at 42.92°, 62.30°, which is due to the high activity of the sample, leading to the slight oxidation during the transportation and measurement process. Based on XRD analysis, it is noted that there is no diffraction peak of carbon detected in the pattern of the MgH_2-CCPA composite, indicating that amorphous carbon may exist in the MgH_2-CCPA composite. The Raman spectra further confirm the presence of amorphous carbon in Fig. 1b. Obviously, there are three principal peaks referred as D-bands, G-bands, and 2D-bands located in the vicinity of 1332.66, 1555.45, 2815.08 cm^{-1}, respectively. The distinct D-bands represent the disorder and irregularity of the carbon material, which cannot be obtained in the Raman spectra of graphene with high crystallinity. The Raman spectra located at 2815.08 cm^{-1} ascribing to 2D-bands further prove the disorder of the as-synthesized material. These analyses confirm the successful preparation of MgH_2-CCPA with amorphous carbon in the composite.

3.2 Hydrogen sorption kinetics

The hydrogen desorption properties of the MgH_2-CCPA composite were identified by the TPD test accompanied by the heating rate of 10 K min^{-1}. It is clearly found that the CCPA had significantly boosted the dehydrogenation of MgH_2 due to the drastic reduction of the onset desorption temperature. The pure MgH_2 starts to release hydrogen at 643 K, with a total hydrogen capacity of 6.561 wt% could be found. The onset temperature for the MgH_2-CCPA composite shifts to a lower temperature compared with the milled MgH_2. The MgH_2-CCPA composite has a decreased onset temperature of about 589 K, which was 54 K lower than that of pure milled MgH_2. Moreover, a higher maximum hydrogen capacity of 6.919 wt% could be detected for the MgH_2-CCPA composite. It is concluded that the hydrogen desorption properties of MgH_2 are dramatically improved by the carbonic combustion product of anthracene.

Further studies concerning the catalytic activity of CCPA on the dehydrogenation of MgH_2 were carried out by evaluating the desorption kinetics.[18] The isothermal hydrogen desorption kinetic curves of the MgH_2-CCPA composite at 623 K and 573 K are presented in Fig. 2b. As a comparison, the dehydrogenation of as-milled MgH_2 was also undertaken under the same condition. It can be clearly seen that the CCPA significantly alters the hydrogen desorption kinetics. Meanwhile, the dehydrogenated MgH_2-CCPA composite shows faster desorption than the undoped MgH_2. The results show that the as-milled MgH_2 desorbs about 3.970 wt% hydrogen after 3000 s of dehydrogenation at 623 K, whereas the MgH_2-CCPA composite

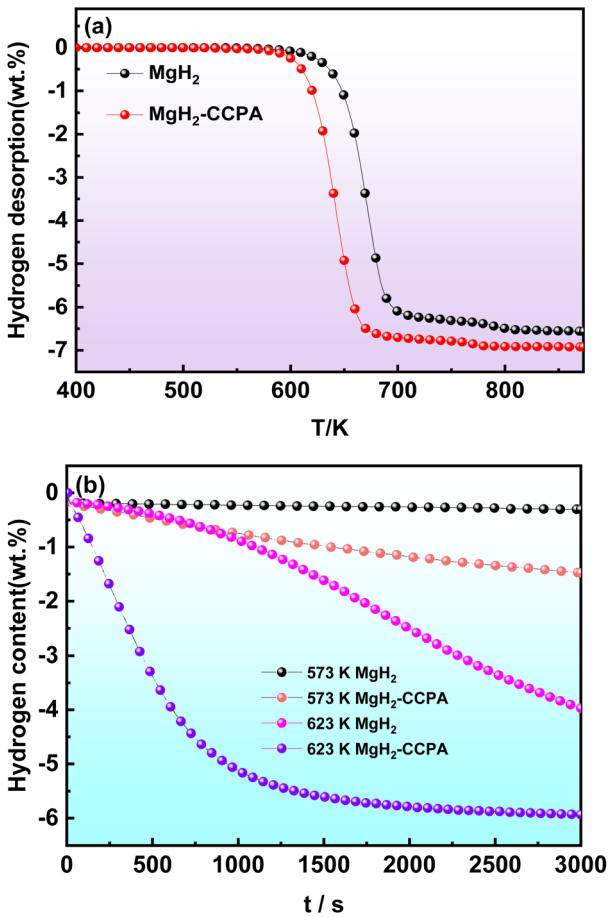

Fig. 2 (a) TPD curves of MgH_2 and MgH_2-CCPA composite; (b) isothermal desorption curves of MgH_2 and MgH_2-CCPA composite at 573 K and 623 K under 0.001 MPa.

makes a significant improvement and about 5.933 wt% hydrogen after 3000 s of dehydrogenation can be desorbed at 623 K in the same period of time. Meanwhile, lowering the temperature to 573 K leads to a slight decrease in the capacity and lower hydrogenation rates than those presented by the samples at 623 K. When the temperature decreases to 573 K, the hydrogen released for MgH_2-CCPA composite is reduced to 1.476 wt% after 3000 s. In contrast, almost no hydrogen could be released by the as-milled MgH_2, and only 0.303 wt% hydrogen was released for as-milled MgH_2 at this temperature in 3000 s. As mentioned above, it is obvious that CCPA plays a crucial role in boosting the dehydrogenation kinetics of MgH_2.

The apparent activation energy of the dehydrogenation (E_a) is a vital parameter that reflects the hydrogen desorption kinetics. The reduced apparent activation energy is correlated to the dehydrogenation reactive barrier for the hydrogen released from MgH_2, which is confirmed by the improved hydrogen desorption kinetics. The apparent activation energy (E_a) values for the sample are calculated by the Kissinger method:[19]

$$\frac{d\left[\ln\left(\alpha/T_m^2\right)\right]}{d\left(1/T_m\right)} = \frac{-E_a}{R} \quad (1)$$

where α is the different heating rate (K min^{-1}), T_m is the peak temperature (K) of dehydrogenation in Fig. 3, and R is the gas constant (8.314 J mol^{-1} K^{-1}). It is evident that the peak temperature for MgH_2-CCPA composite catalyst is much lower than that of pure MgH_2 at the same heating rate.

Fig. 3 shows DSC curves for the as-milled MgH_2 and MgH_2-CCPA composite at the heating rate of 5, 10, 15, 20 K min^{-1}. With the increase in the heating rate from 5 K min^{-1} to 20 K min^{-1}, the peak temperature is increased. The E_a value for the hydrogen for the MgH_2-CCPA composite is about 77.5 kJ mol^{-1}, which is significantly lower than that of the as-milled MgH_2 (161.1 kJ mol^{-1}). Based on the Kissinger analysis, the reduced dehydrogenation reaction energy barrier is obtained by the MgH_2-CCPA composite, which leads to the facile dehydrogenation process and further boosts the desorption properties of MgH_2.

To further reveal the hydrogen storage behavior of the MgH_2-CCPA composite, the isothermal hydrogenation measurements were conducted at 423 K and 473 K, respectively. As illustrated in the isothermal hydrogenation curves (Fig. 4a), the as-milled MgH_2 can hardly absorb any hydrogen at a temperature as low as 423 K. When the temperature rises to 473 K, only 1.719 wt% of hydrogen can be uptaken by the as-milled MgH_2 at 3000 s, but the hydrogen absorption kinetics is still not satisfying. Nevertheless, MgH_2-CCPA shows significantly improved hydrogen absorption kinetics combined with notably higher

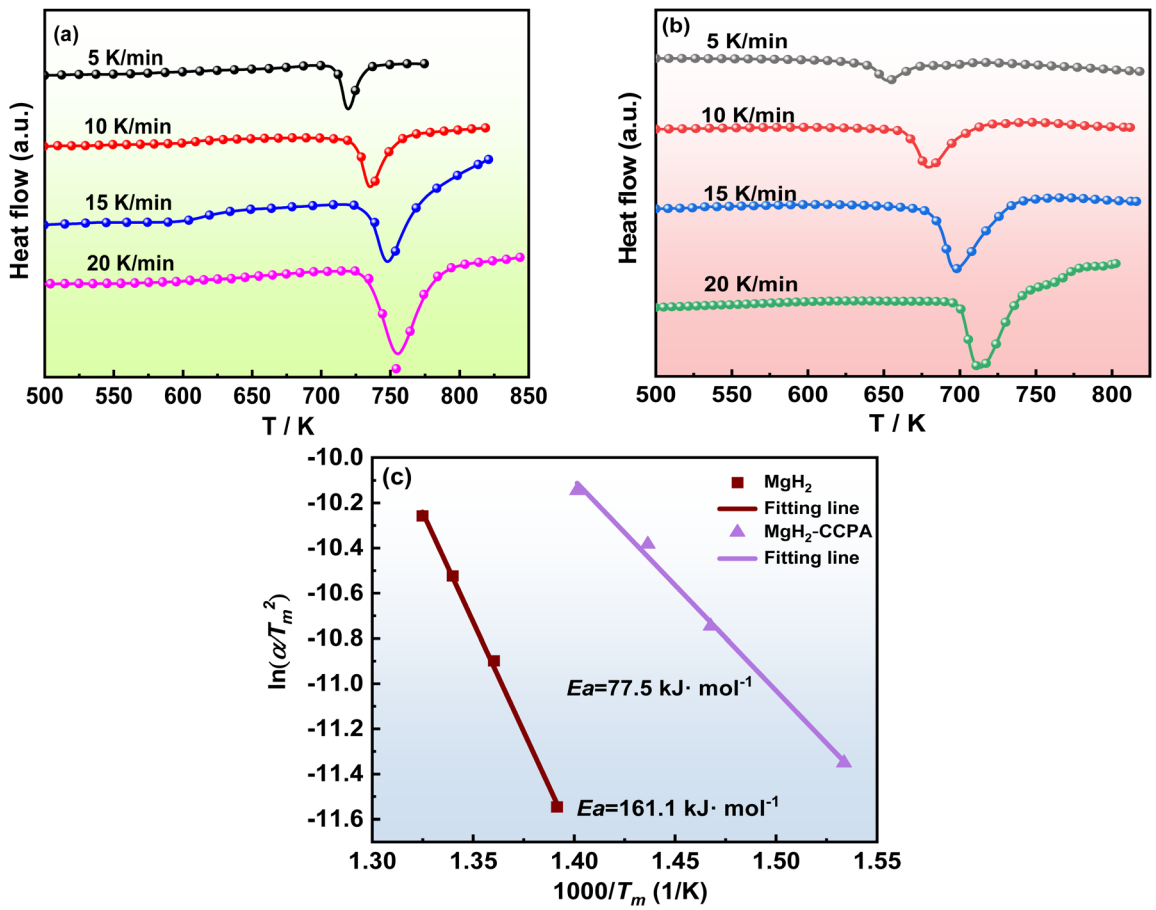

Fig. 3 DSC curves of MgH_2 (a) and MgH_2-CCPA composite (b) at different heating rates; (c) Kissinger's plots for milled MgH_2 and MgH_2-CCPA composite.

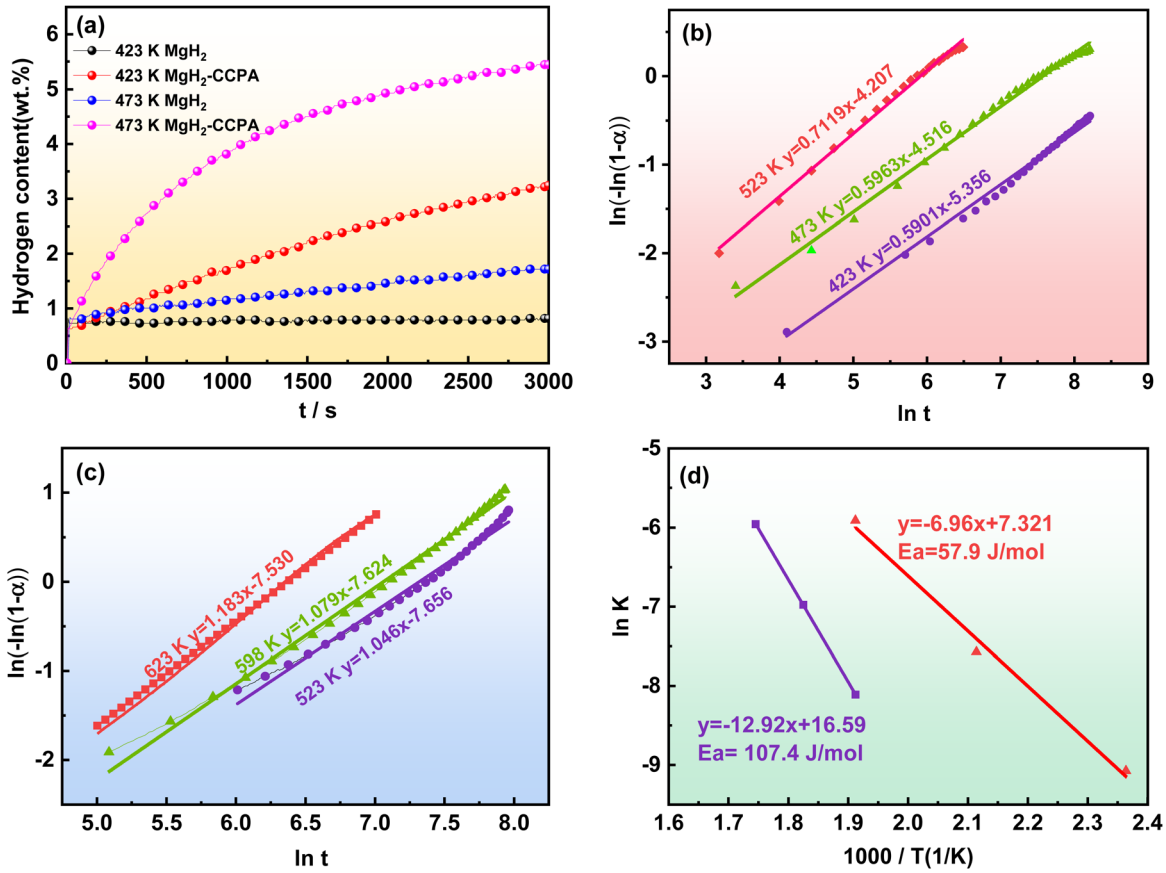

Fig. 4 (a) Isothermal hydrogen absorption curves of MgH_2 and MgH_2-CCPA composite at 423 K and 473 K under 3.0 MPa; (b) rehydrogenation and (c) dehydrogenation; (d) Arrhenius plots for the rehydrogenation of MgH_2-CCPA composite and MgH_2.

hydrogen capacity than the as-milled MgH_2. With an increase in the temperature from 423 K to 473 K, the kinetic properties of hydrogen absorption and capacity for the MgH_2-CCPA composite rise dramatically, which is confirmed by many research studies that the rising temperature favors the promotion of the hydrogenation ability.[20] At 423 K, the MgH_2-CCPA composite can quickly absorb 1.694 wt% of hydrogen within 1000 s and reach a capacity of 3.246 wt% within 3000 s, three times higher than the pure MgH_2 (0.818 wt%) at the same time. The excellent hydrogen absorption and hydrogen rate could also be found at a higher temperature, and the hydrogen uptake at 473 K can be even rapidly absorbed at 5.416 wt% of hydrogen within 3000 s; this exceeds about two times for the pristine MgH_2 at the same temperature. Table 1 also illustrates the hydrogen absorption properties for several recently reported MgH_2 systems with carbon materials as catalysts. It can be concluded that the introduction of CCPA can make the MgH_2 system obtain relatively excellent hydrogen sorption kinetics.

In order to further explain the hydrogen absorption mechanism of the MgH_2-CCPA composite, the hydrogen absorption curves for these samples were fitted by the Johnson–Mehl–Avrami (JMA) model and Arrhenius analysis by fitting the absorption curves of MgH_2, which helps to understand the hydrogenation absorption/desorption process mechanism and dimensionality of MgH_2. The equation can be described as follows:[25]

$$\ln[-\ln(1-\alpha)] = n\ln k + n\ln t \quad (2)$$

where α refers to the reactive extent of the composite at time t, k represents the rate constant, and the Avrami exponent n can be used to depict the dimensionality of the growth process and the information about the rate-limiting step of the reaction. The sorption curves at different temperatures are fitted by $\ln(-\ln(1-\alpha))$ *vs.* $\ln t$, and the hydrogen absorption activation energy is obtained by the slope of the fitting line.

Obviously, it could be noted that the $\ln[\ln(1-\alpha(t))]$ has a good straight line against $\ln(t)$ when α varies from 0.2 to 0.8, which indicates the hydrogen sorption of MgH_2-CCPA composites is in accordance with the JMA model. The Avrami exponent n in the hydrogen absorption process for the MgH_2-CCPA composites are taken as 0.5901 at 423 K and 0.5963 at 473 K and continuously moves to 0.7119 at 523 K. The Avrami exponent n for the tested temperature is close to 0.5 and far away from 1, which exhibits that the hydrogenation process can be explained by the hydrogen diffusion mechanism for the MgH_2-CCPA composite. It is observed that the hydrogen desorption curves at 573, 598, and 623 K also provide an excellent linear relationship, and the corresponding Avrami

Table 1 Comparative study of the hydrogen properties of MgH_2-based hydrogen storage materials

Sample	Synthesis method	Hydrogen pressure, capacity	Reference
MgH_2@AC	Hydrogenation	2 MPa, 10 min, 3.2 wt%	11
MgH_2@G	Hydrogenation	2 MPa, 10 min, 4.0 wt%	11
MgH_2-CCS	Hydrogenation	2 MPa, 10 min, 5.2 wt%	11
MgH_2-CA	Hydrogenation	3 MPa, 1000 s, 0.56 wt%	11
MgH_2@BCNTs	Ball milling	8 MPa, 10 min, 5.9 wt%	21
$Mg_{85}Al_{15}$ + V_2O_5@rGO	Hydrogenation	8 MPa, 1500 s, 4.23 wt%	22
MgH_2-Co@C	Ball milling	5 MPa, 600 s, 5.96 wt%	23
MgH_2-Nb@C	Ball milling	4 MPa, 5 min, 5.6 wt%	24
MgH_2@C	Hydrogenation	4 MPa, 20 min, 4.8 wt%	24
MgH_2-CCPA	Hydrogenation	3 MPa, 300 s, 6.62 wt%	This work

exponent n values of dehydrogenation for the tested temperatures are 1.046, 1.079, and 1.183, respectively. All the Avrami exponent n values in the tested temperatures approach 1, implying that the dehydrogenation process of MgH_2-CCPA composite ascribes to one-dimensional with interface-controlled growth theory.[26] According to the Avrami exponent value, the rate-limiting process of hydrogenation and dehydrogenation lies in the diffusion and the interface-controlled growth through the hydride. Further comparing the hydrogen absorption activation energy for the MgH_2-CCPA composite with as-milled MgH_2, the hydrogen absorption activation energy for the MgH_2-CCPA composites is proved to be 57.9 kJ mol^{-1}, which is almost 49.5 kJ mol^{-1} lower than the pristine MgH_2 in the hydrogen uptaken process. The reduced hydrogen absorption activation energy is beneficial to the improved hydrogen absorption amount and accelerates the hydrogenation/dehydrogenation rate due to the CCPA modification. The introduced CCPA is highly efficacious in decreasing the hydrogen absorption activation energy for MgH_2 and thus enhances the hydrogen absorption kinetics of MgH_2.

As mentioned above, the MgH_2-CCPA composite exhibits brilliant de/absorption kinetics on the first hydrogenation/dehydrogenation measurement, while excellent recyclability, reproducibility, and long-term sustainability are significantly vital for practical application. The above samples after the hydrogen absorption and desorption process were stored in vacuum, and their hydrogen sorption performance was measured three months later. Fig. 5 exhibits the cycling de/absorption curves of the MgH_2-CCPA composite 10 times at 623 K. It is worth noting that the hydrogen de/absorption content of MgH_2-CCPA was maintained at 98% after 10 cycles. Moreover, no evident capacity decline can be detected, confirming that the carbonized modification shows a significant promotion for the cyclic stability, reproducibility, and long-term sustainability of MgH_2.

3.3 Catalytic mechanism

To clearly understand the phase changes of the MgH_2-CCPA composite during the different stages, XRD analysis was carried out to investigate the phase constitution of the MgH_2-CCPA composite. Fig. 6 shows the XRD patterns of the ball-milled, hydrogenation, and dehydrogenation states. The diffraction peak in the ball-milling process is extremely short and wide; it can be observed that the primary diffraction peak for the ball-milled process is MgH_2, while some small peaks corresponding to MgO are also detected in this pattern. No other new phases are detected in the XRD pattern, as shown in Fig. 6A(a). Fig. 6A(b) presents the XRD patterns of the re-hydrogenated composites at 623 K under the hydrogen pressure at 3.0 MPa. Clearly, the diffraction peaks of MgH_2 and MgO are still observed in this state. Moreover, the diffraction peak of the re-hydrogenated sample is much higher than that of the ball-milled sample, which is mainly due to the elimination of the micro-strain and the recrystallization of the samples during re-hydrogenation process.[27,28] There exists a primary phase transformation between MgH_2 and Mg during the dehydrogenated process, and MgH_2 is completely dehydrogenated to Mg. The diffraction peaks of Mg are clearly identified, accompanied by the disappearance of the MgH_2 peaks. Moreover, the MgO diffraction peak clearly remains unchanged in the whole process, which is attributed to the fact that the XRD tests are not completely isolated from air, and oxidation is inevitable. No diffraction peak assigned to carbon or carbon-containing phase could be found by XRD in the ball-milling process, suggesting that carbon existed in an

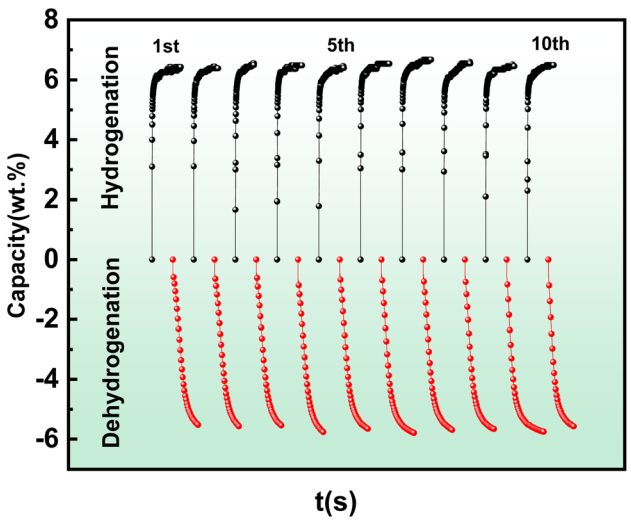

Fig. 5 Cycling hydrogen sorption curves of MgH_2-CCPA composite for 10 times at 623 K.

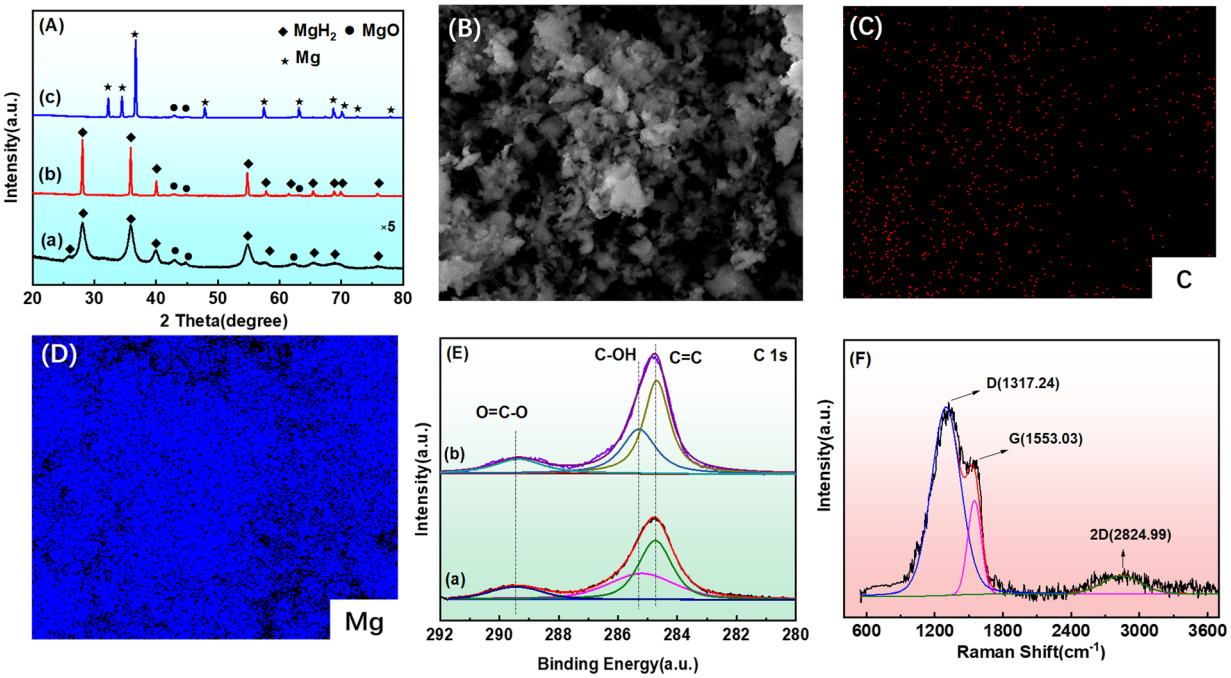

Fig. 6 (A) XRD spectrum of as-synthesized MgH_2-CCPA composite: (a) ball milled; (b) hydrogenation; (c) dehydrogenation; (B) SEM images of the hydrogenated MgH_2-CCPA composite with the mapping of C (C) and Mg (D); (E) C1s XPS spectra of the hydrogenation (a) and dehydrogenation (b) of the MgH_2-CCPA composite; (F) Raman spectra of the hydrogenated MgH_2-CCPA composite.

amorphous structure combined with the analysis in Fig. 1. Meanwhile, SEM confirms that the MgH_2-CCPA composite shows less agglomeration (Fig. 6B) and the uniform distribution of C elements are observed from EDS mapping (Fig. 6(C and D)). The C element state is confirmed by the XPS from Fig. 6E, and the peaks at 284.7 eV, 285.3 eV, and 289.4 eV in the C1s spectra are ascribed to C–C, C–OH, and O=C–C bonds. The new C–OH and O=C–C bonds indicate the formation of additional carbon in the MgH_2-CCPA composites. Combined with the Raman analysis (Fig. 6F), three dominant peaks corresponding to D-bands, G-bands, and 2D-bands could be detected. The distinct D-bands refer to the disorder and irregularity of the carbon material, which cannot be obtained in the Raman spectra of graphene with high crystallinity. The Raman spectra located at 2824.99 cm^{-1} ascribed to 2D-bands further prove the disorder of the as-synthesized material. This analysis exhibits the existence of the amorphous carbon in the whole process of the composite, which acted as the real activated phase for the enhancement of hydrogen storage for the as-milled MgH_2.

Combining the above analysis, the improved hydrogen sorption kinetics of MgH_2 by adding CCPA are speculated to those factors, and the corresponding mechanism is described in Fig. 7: after sintering at a high temperature of 873 K, the pyrolysis of anthracene produces amorphous carbon with numerous defects, which is evenly distributed on the surface of the Mg particles. During the ball-milling process, the amorphous carbon plays a vital role in inhibiting the crystal growth and the agglomeration of particles, which is beneficial for the improvement of the hydrogen sorption behavior. As reported by Rud *et al.*,[29] the amorphous carbon promotes more fine

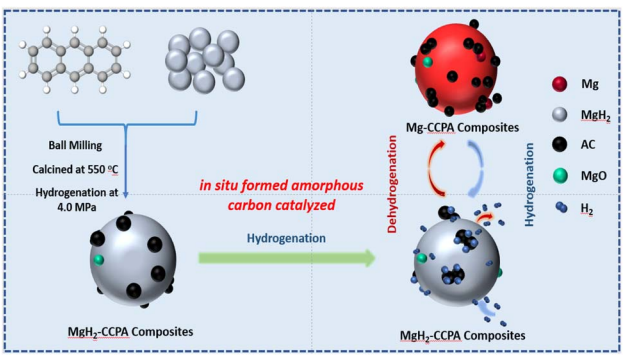

Fig. 7 The mechanism diagram for the MgH_2-CCPA composites.

pulverization of magnesium under the ball milling process, which results in a significant increase in hydrogen sorption rate for the magnesium. In the hydrogenation/dehydrogenation process, the amorphous carbon in MgH_2-CCPA composites provides more active sites and further shortens the distance of the H diffusion, which dramatically reduces the sorption energy value of H in MgH_2 and significantly accelerates the hydrogen storage kinetics of MgH_2.[30] More importantly, the *in situ* formed catalysts in the Mg matrix show better catalytic effects than the catalysts added by ball milling.[31]

4 Conclusions

The present work is focused on the synthesis of amorphous carbon through the carbonic combustion product of anthracene

with MgH_2. The *in situ* formed amorphous carbon derived from the carbonic combustion product of anthracene plays an important role in the improvement of the hydrogen sorption behavior of the MgH_2-CCPA composite. The hydrogen absorption capacity for MgH_2-CCPA composite is 3.246 wt% at 423 K for 3000 s, which is higher compared to undoped MgH_2 that had uptaken 0.818 wt% during the same period. The MgH_2-CCPA composites exhibit an unexpected high-efficient catalytic activity for dehydrogenation properties of MgH_2, causing the release of approximately 5.933 wt% of hydrogen at 623 K after 3000 s; meanwhile, the as-milled MgH_2 only released 3.970 wt% under similar conditions. The initial decomposition temperature for the MgH_2-CCPA composite is about 589 K, which was 54 K lower than that of pure milled MgH_2. Moreover, the E_a value of hydrogen for the MgH_2-CCPA composite is about 77.5 kJ mol^{-1}, which is significantly lower than that of the as-milled MgH_2 (161.1 kJ mol^{-1}). From the above, the significantly improved hydrogen sorption properties of MgH_2-CCPA can be attributed to the *in situ* formation of amorphous carbon, which plays the catalytic role in the improvement of MgH_2.

Conflicts of interest

There are no conflicts to declare.

Acknowledgements

This work was supported by the Natural Science Foundation of China (22202058); Science and Technology Project of Hebei Education Department (BJ2020043); Hebei University of Environmental Engineering (Top-notch Talents Cultivation Program for Young Science and Technology 2020ZRBJ01); Doctoral Foundation of Hebei University of Environmental Engineering (201805).

Notes and references

1 Y. H. Zhang, H. F. Sun, W. Zhang, Z. M. Yuan, X. Wei, J. L. Gao and H. P. Ren, *Int. J. Hydrogen Energy*, 2021, **46**, 28719–28733.
2 P. Pal, S. Agarwal, A. Tiwari, T. Ichikawa, A. Jain and A. Dixit, *Int. J. Hydrogen Energy*, 2022, **47**, 41891–41897.
3 N. N. Sulaiman, N. S. Mustafa and M. Ismail, *Dalton Trans.*, 2016, **45**, 7085–7093.
4 M. Song, L. Zhang, Z. Yao, J. Zheng, D. Shang, L. Chen and H. Li, *Inorg. Chem. Front.*, 2022, **9**, 3874–3884.
5 S. Dong, C. Li, J. Wang, H. Liu, Z. Ding, Z. Gao, W. Yang, W. Lv, L. Wei, Y. Wu and H. Li, *J. Mater. Chem. A*, 2022, **10**, 22363–22372.
6 N. Nyamsi, Z. Wu, Z. X. Zhang, A. Kolesnikov, M. V. Lototskyy and S. Pasupathi, *Appl. Therm. Eng.*, 2022, **209**, 118314–118329.
7 X. Feng, L. Jiang, Z. Li, S. Wang, J. Ye, Y. Wu and B. Yuan, *Int. J. Hydrogen Energy*, 2022, **47**, 23994–24003.
8 W. Zhu, L. Ren, C. Lu, H. Xu, F. Sun, Z. Ma and J. Zou, *ACS Nano*, 2021, **15**, 18494–18504.
9 X. Zhang, Y. Liu, Z. Ren, X. Zhang, J. Hu, Z. Huang, Y. Lu, M. Gao and H. Pan, *Energy Environ. Sci.*, 2021, **14**, 2302–2313.
10 X. Zhang, K. Wang, X. Zhang, J. Hu, M. Gao, H. Pan and Y. Liu, *Int. J. Energy Res.*, 2021, **45**, 3129–3141.
11 Q. Zhang, Y. Huang, T. Ma, K. Li, F. Ye, X. Wang, L. Jiao, H. Yuan and Y. Wang, *J. Alloys Compd.*, 2020, **825**, 153953.
12 Y. Zhao, Y. Zhu, J. Liu, Z. Ma, J. Zhang, Y. Liu, Y. Li and L. Li, *J. Alloys Compd.*, 2021, **862**, 158004–158011.
13 M. Zhang, X. Z. Xiao, B. S. Luo, M. J. Liu, M. Chen and L. X. Chen, *J. Energy Chem.*, 2020, **46**, 191–198.
14 A. D. Rud and A. M. Lakhnik, *Int. J. Hydrogen Energy*, 2012, **37**, 4179–4187.
15 S. Wang, M. Gao, K. Xian, Z. Li, Y. Shen, Z. Yao, Y. Liu and H. Pan, *ACS Appl. Energy Mater.*, 2020, **3**, 3928–3938.
16 Y. F. Zhu, W. F. Zhang, C. Yang and L. Q. Li, *Int. J. Hydrogen Energy*, 2010, **35**, 9653–9660.
17 X. Xie, X. Ma, P. Liu, J. Shang, X. Li and T. Liu, *ACS Appl. Mater. Interfaces*, 2017, **9**, 5937–5946.
18 M. Ismail, N. S. Mustafa, N. Juahir and F. A. H. Yap, *Mater. Chem. Phys.*, 2016, **170**, 77–82.
19 X. L. Yang, Q. H. Hou, L. B. Yu and J. Q. Zhang, *Dalton Trans.*, 2021, **50**, 1797–1807.
20 N. S. Mustafa and M. Ismail, *J. Alloys Compd.*, 2017, **695**, 2532–2538.
21 M. Liu, S. Zhao, X. Xiao, M. Chen, C. Sun, Z. Yao, Z. Hu and L. Chen, *Nano Energy*, 2019, **61**, 540–549.
22 J. Du, Z. Lan, H. Zhang, S. Lu, H. Liu and J. Guo, *J. Alloys Compd.*, 2019, **802**, 660–667.
23 L. Li, G. X. Jiang, H. R. Tian and Y. J. Wang, *Int. J. Hydrogen Energy*, 2017, **42**, 28464–28472.
24 C. Zhu, M. Chen, M. Hu, D. He, Y. Liu and T. Liu, *Int. J. Hydrogen Energy*, 2021, **46**, 9443–9451.
25 M. Chen, M. Hu, X. Xie and T. Liu, *Nanoscale*, 2019, **11**, 10045–10055.
26 Z. X. Wang, Z. H. Tian, P. F. Yao, H. M. Zhao, C. Q. Xia and T. Yang, *Renewable Energy*, 2022, **189**, 559–569.
27 N. Lobo, A. Takasaki, K. Mineo, A. Klimkowicz and K. Goc, *Int. J. Hydrogen Energy*, 2019, **44**, 29179–29188.
28 J. G. Yuan, N. Xing and Y. Wu, *Int. J. Hydrogen Energy*, 2017, **42**, 6118–6126.
29 A. D. Rud and A. M. Lakhnik, *Int. J. Hydrogen Energy*, 2012, **37**, 4179–4187.
30 M. Zhang, X. Xiao, J. Mao, Z. Lan, X. Huang, Y. Lu, B. Luo, M. Liu, M. Chen and L. Chen, *Mater. Today Energy*, 2019, **12**, 146–154.
31 L. Z. Ouyang, X. S. Yang, M. Zhu, J. W. Liu, H. W. Dong, D. L. Sun, J. Zou and X. D. Yao, *J. Phys. Chem. C*, 2014, **118**, 7808–7820.